1
Resonances and Mixing in Near-Integrable Volume-Preserving Systems

Dmitri Vainchtein

1.1
Introduction

Many laminar flows are often characterized by a high degree of symmetry due to the confining effect of surface tension (for free-surface flows, e.g., in microdroplets) and/or device geometry (e.g., for flows in microchannels). Designing a flow with good mixing properties is particularly difficult in the presence of symmetries. Symmetry leads to the existence of (flow) *invariants* [1, 2], which are functions of coordinates that are constant along streamlines of the flow. The level sets of one invariant define surfaces on which the (three-dimensional) flow is effectively two-dimensional. An additional invariant further reduces the flow dimensionality: a flow with two invariants is effectively one-dimensional. Since the flow cannot cross invariant surfaces, the existence of invariants is highly undesirable in the mixing problem as their presence inhibits complete stirring of the full fluid volume by advection. Neither is chaotic advection per se sufficient for good mixing, as time-dependent flows [3, 4] can have chaotic streamlines restricted to two-dimensional surfaces in the presence of an invariant. Thus, the key to achieving effective chaotic mixing in any laminar flow is to ensure that all flow invariants are destroyed.

In this section we will focus on the class of laminar flows characterized by small deviations from exact symmetries. Not only are such flows common in various applications of microfluidics, this is *the only* class of flows that generically affords a quantitative analytical treatment. The description of the weakly perturbed flow in terms of the action and angle variables allows quantitative analytical treatment using perturbation theory. Indeed, if the symmetries are broken weakly, the invariants (or actions) of the unperturbed flow become slowly varying functions of time (start to *drift*, in the more technical language) for the perturbed flow, while the angle variable remains quickly varying. Such perturbed flows are referred to as *near-integrable*, in contrast to the flows with exact symmetries which are *integrable*, that is, possess an exact analytical solution. Near-integrable systems play a prominent role in many areas of science. Often they arise naturally when there is a large separation of scales and, hence, of the associated forces, for example, as in many problems in celestial

Transport and Mixing in Laminar Flows: From Microfluidics to Oceanic Currents,
First Edition. Edited by Roman Grigoriev.

mechanics, where the gravitational interaction with the Sun dominates all other forces which can be considered small perturbations [5, 6]. Similarly, for weakly perturbed action–action–angle fluid flows there is a large separation of timescales on which the actions and the angle change.

The space of the integrable unperturbed system is foliated into invariant tori and the motion on these tori is quasi-periodic or periodic. If there are two independent integrals, the tori are invariant closed curves. In general, the integrability requires the existence of at least one *conserved quantity* (or *action* or *invariant*), so all flows of interest belong to one of two classes: action–action–angle or action–angle–angle [1]. Transport in the perturbed action–angle–angle flows is severely restricted by KAM tori (it was illustrated in [7]), while the effective degeneracy of the action–action–angle flows opens the possibility of global transport and mixing. We will, therefore, focus our attention on action–action–angle flows and possible mechanisms leading to chaotic advection.

Exact analytic solutions for near-integrable dynamics cannot be obtained. Direct brute-force numerical simulation of such systems is possible, but usually very challenging precisely due to a big separation of timescales. Approximate analytical tools represent an important alternative for studying such systems. Specifically, the assumption of a weak perturbation allows one to use a collection of perturbation theory methods to describe the dynamics quantitatively. In particular, by averaging the evolution equations for the actions I and J over a period of the fast motion described by the angle ϕ one finds that although the original exact invariants are destroyed, the averaged system of equations itself possesses an invariant $\Phi(I, J)$. Since the averaged equations are an approximation, in the exact perturbed system Φ is only conserved in the adiabatic sense: its value undergoes small oscillations with period close to that of ϕ but the average value of Φ remains the same on much longer time intervals [8]. Therefore, this approximate invariant is referred to as an *adiabatic invariant* (AI).

As it turns out, the existence of an AI enables a greatly simplified description of the mixing dynamics in near-integrable flows. Of course, if the AI were conserved everywhere, mixing would be restricted to the two-dimensional level sets of the AI (usually tori) defined by $\Phi = \text{const}$, which is often indeed the case (i.e., nonintegrability does not lead to mixing). Mixing requires the breakdown of the adiabatic invariance, which can occur in the flows possessing certain types of *singular manifolds*, where the fast subsystem slows down and the separation of scales disappears. A very elegant description of the dynamics can be obtained by separating the evolution into regular advection along the 2D level sets of the AI *between* singular manifolds, and fast passages *through* the singular manifolds. During the motion near the singular manifolds, the value of the AI typically experiences a change that is much larger than the magnitude of the oscillations of the AI during the motion far from the singular manifolds. As the time of the passage near the singular manifolds is much shorter than the characteristic time of motion between them, the changes in the AI can be treated as instantaneous *jumps* in describing the evolution of the AI. For every set of initial conditions, the magnitude of the jump in the AI can be calculated exactly.

However, a small change in the initial conditions produces in general a large change in the jump magnitude [9, 10]. Hence, for weak perturbations, in computing the statistical properties of many consequent jumps, it is possible to treat the jump magnitude as a random variable with statistical properties obtained from the dependence of the jump magnitude on initial conditions. The dynamics in the vicinity of singular manifolds (separatrices or resonance surfaces) can be described using a different perturbation expansion, where the small parameters are not just the perturbation strength but also the distance to the singular manifold. For resonant surfaces, this approach was first introduced in [11, 12] and further developed in [10, 13] in the context of Hamiltonian systems and subsequently applied to 3D volume-preserving autonomous (such as flows of incompressible fluids) in [14] and nonautonomous [4] systems. A theory for systems with separatrix crossings was proposed in [15, 16] and later developed in [17–19] for Hamiltonian systems and in [9, 20] for 3D volume-preserving autonomous systems.

If allowed by the geometry of the system, the streamline keeps coming to the singular surface(s) again and again and the process of jumps repeats itself. Accumulation of jumps at multiple crossings results in destruction of the adiabatic invariance (i.e., the AI changes by a value of the order 1) and leads to chaotic dynamics in the system. Therefore, the physical space becomes partitioned into the domains of chaotic and regular dynamics filled, respectively, by the streamlines that do, or do not, cross the singular manifold(s). In the chaotic domain, the jumps of the AI associated with separatrix or resonance crossings lead to the destruction of adiabatic invariance and transport across the level sets of the AI. Over long timescales, accumulation of small jumps coupled with the divergence of initially close streamlines lead to effective diffusion of the AI and mixing. This dynamical picture allows one to compute the size and shape of the chaotic and regular domains and to estimate the rate of mixing.

The theory of long-time transport in volume-preserving flows in the presence of chaotic advection and regular diffusion is by no means limited to mixing in fluid flows [21–25]. Such a description of long-time transport in near-integrable Hamiltonian and volume-preserving systems is crucial for long-term predictions of, for example, the dynamics of comets and asteroids [26–28], customizing transport to achieve selective segregation in electromagnetic diverters in plasma confinement devices [29–31], energy exchange between coupled oscillators [32–34], chaotic billiards [35], arrays of Josephson junctions [36, 37], and the drift of charged particles in the Earth magnetosphere [38–42].

In this chapter, we describe destruction of AIs at separatrices and resonances and use several examples studied earlier [4, 14, 43, 44] to illustrate different aspects of the complete picture. We refer the reader to the corresponding chapter for details of derivations and additional discussions. General properties are discussed in Section 1.2. Separatrix crossings are discussed in Section 1.3, and passages through resonances in autonomous and nonautonomous flows are considered in Sections 1.4 and 1.5, respectively.

1.2 General Properties of Near-Integrable Flows and Different Types of the Resonance Surfaces

The motion of passive tracers advected by the flow can be described by a volume-preserving system of ODE in $\mathbf{R}^3$ depending on a small parameter, $0 < \varepsilon \ll 1$:

$$\dot{\mathbf{x}} = \mathbf{v}(\mathbf{x}) + \varepsilon \mathbf{w}(\mathbf{x}, t, \varepsilon), \qquad \operatorname{div} \mathbf{v} = \operatorname{div} \mathbf{w} = 0 \tag{1.1}$$

Velocity field $\mathbf{v}$ in (1.1) defines an unperturbed (base) flow; $\mathbf{w}$ is a perturbation and is supposed to be a smooth function of ε. We restrict our discussion to 3D autonomous base flows, while the perturbation may be autonomous or nonautonomous. System (1.1) at $\varepsilon = 0$ corresponds to the unperturbed system. In a sense, passive tracers in the flows are equivalent to phase points in generic dynamical systems.

The effects of the small perturbation in (1.1) start manifesting themselves on time intervals of order at least ε^{-1}. A function of phase variables is called an AI if its value along a phase trajectory of (1.1) has only small (with ε) variations on time intervals of such length. In other words, an AI is an approximate first integral of the system. Perpetual conservation of AI presents a barrier for complete mixing.

Let unperturbed system (1.1) be integrable and of the action–action–angle type. Then, almost the entire phase space is filled with closed streamlines. Denote the two independent integrals of motion as I and J. Every joint level of the two integrals $I = i$, $J = j$ defines a closed unperturbed phase trajectory $\Gamma_{i,j}$. Introduce on $\Gamma_{i,j}$ an angular variable ϕ mod 2π changing at a constant rate in the unperturbed motion.

The perturbation in (1.1) causes the values of I and J to change at a rate of order ε in the motion along a perturbed streamline. In terms of the variables i, j, ϕ, perturbed system (1.1) can be written as

$$\frac{\mathrm{d}i}{\mathrm{d}t} = \varepsilon f(i,j,\phi,\varepsilon) \quad \frac{\mathrm{d}j}{\mathrm{d}t} = \varepsilon g(i,j,\phi,\varepsilon) \quad \frac{\mathrm{d}\phi}{\mathrm{d}t} = \Omega(i,j) + \varepsilon h(i,j,\phi,\varepsilon) \tag{1.2}$$

The functions f, g, h are 2π-periodic in ϕ. In (1.2), the variables i, j are "slow," and the variable ϕ is "fast." Define the averaged system:

$$\frac{\mathrm{d}i}{\mathrm{d}t} = \varepsilon F(i,j) \quad \frac{\mathrm{d}j}{\mathrm{d}t} = \varepsilon G(i,j) \tag{1.3}$$

where functions F and G are obtained by averaging f and g, respectively, over ϕ:

$$F(i,j) = \frac{1}{2\pi}\int_{\Gamma_{i,j}} (\operatorname{grad} I, \mathbf{w})\, \mathrm{d}\phi \quad G(i,j) = \frac{1}{2\pi}\int_{\Gamma_{i,j}} (\operatorname{grad} J, \mathbf{w})\, \mathrm{d}\phi \tag{1.4}$$

In (1.4), $\mathbf{w}$ is calculated at $\varepsilon = 0$, parentheses denote the scalar product, and the integration is performed along $\Gamma_{i,j}$. Far from the singular surfaces (described below), solutions of the averaged system describe variations of i, j in complete system (1.1) with the accuracy of order ε on time intervals of order ε^{-1} [45, 46].

Let $\Phi(i,j)$ be the flux of the perturbation through a surface spanning $\Gamma_{i,j}$. Due to the preservation of the volume, the value of $\Phi(i,j)$ does not depend on a particular choice of the surface. A remarkable fact is that averaged system (1.3) is Hamiltonian, and

$\Phi(i,j)$ is a Hamiltonian function (see, e.g., [9, 20]):

$$\frac{\mathrm{d}i}{\mathrm{d}t} = \frac{\varepsilon}{\mu(i,j)T(i,j)}\frac{\partial\Phi(i,j)}{\partial j} \quad \frac{\mathrm{d}j}{\mathrm{d}t} = -\frac{\varepsilon}{\mu(i,j)T(i,j)}\frac{\partial\Phi(i,j)}{\partial i} \tag{1.5}$$

where $\mu(i,j)$ is a certain function of i and j, determined by the base flow and $T(i,j) = 2\pi/\Omega(i,j)$ is the period of the unperturbed motion along $\Gamma_{i,j}$. In almost all the systems we studied recently, $\mu(i,j) \equiv 1$. Moreover, it is always the case when the base flow has axial symmetry and the two invariants are the streamfunction and the azimuthal angle. It follows from (1.5) that $\Phi(i,j)$ is an integral of the averaged system. Standard assertions about the accuracy of the averaging method (see, e.g., [8, 45, 46]) imply that Φ is an approximate integral of the motion in exact system (1.1), that is, Φ is an *adiabatic invariant* (see Figure 1.1a below).

However, the averaging method breaks down in a neighborhood of 2D *singular surfaces*. These surfaces can be of one of three types:

1) *Separatrix surfaces* containing nondegenerated hyperbolic fixed points of the unperturbed system and filled by heteroclinic trajectories connecting them. A systems of this type is considered in Section 1.3.
2) *Separatrix surfaces* containing a line of degenerate singular points (this case occurs, in particular, in 1 d.o.f. Hamiltonian systems depending on a slowly varying parameter or a no-autonomous flows with axial symmetry, and it is considered elsewhere [15, 16, 47]).
3) *Resonance surfaces*, corresponding to closed curves filling a surface. In *autonomous* systems with one angle variable, the function $\Omega(i,j)$ in (1.2) is identically zero everywhere on such a surface. A system of this type is considered in Section 1.4. In *nonautonomous* systems in which time appears as an additional fast phase with a frequency ω, on resonance surface $\Omega(i,j)/\omega$ is a rational number (see Section 1.5). The major difference between separatrix and resonance surfaces is that near separatrix surfaces the base flow slows down only in

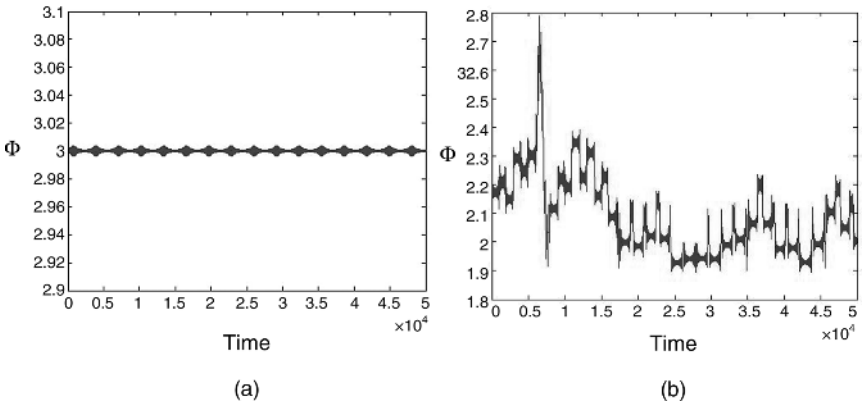

Figure 1.1 Adiabatic invariants (a) away from the singular surfaces and (b) when a streamline crosses them. The model from [14].

the immediate vicinity of fixed points of the base system. In comparison, a linear combination (with integer coefficients) of the phase of the base flow and the time variable slows down everywhere near a resonance surface.

Let us just briefly note that the problem of jumps of AIs at separatrix crossings in volume-preserving systems cannot be reduced to similar problems in Hamiltonian systems depending on a slowly varying parameter [15, 16, 47], or in slow–fast Hamiltonian systems [48]. Although ideologically close to them, this problem needs an independent study. Similar phenomena were also observed in 3D volume-preserving maps [7].

A complete description of chaotic advection in these problems starts with a description of a *single crossing* of a resonance or a separatrix surface. Let a phase point (passive tracer) $i(t), j(t)$ closely follow a trajectory of the averaged system. The quantity $\Phi(i, j)$ along the streamline oscillates with an amplitude of order ε around a certain constant value, say, Φ_1. When the streamline crosses a small neighborhood of a singular surface, Φ changes by a value $\Delta\Phi \sim \varepsilon^{\alpha}$, $0 < \alpha < 1$, which is in general much greater than ε. In the case of scatterings on resonance and almost all the separatrix crossings, $\alpha = 1/2$. After this neighborhood is crossed, the value of Φ along the trajectory oscillates near a new constant value, $\Phi_2 = \Phi_1 + \Delta\Phi$. As the main change occurs in a narrow neighborhood of a singular surface, we shall call this change a *jump of the AI*. In every particular problem, an asymptotic formula (in the limit of small values of ε) for this change of the AI can be obtained following a standard procedure which was reported in several publications [4, 9, 20, 43, 44, 49]. An example of such a dynamics is illustrated in (see Figure 1.1b). In the case of crossing a resonance when there is the possibility of capture into resonance, the captured dynamics can be also described.

The magnitude of a jump turns out to be very sensitive to variations of initial conditions. Therefore, the jump is in a sense random. If allowed by the geometry of the system, the streamline comes to the separatrix again and the process repeats itself. Accumulation of jumps at multiple crossings results in destruction of the adiabatic invariance (i.e., the AI changes by a value of the order 1) and leads to chaotic dynamics in the system. Based on the equations for a single passage, we can describe statistical properties of jumps and use them to study the long-time dynamics on time intervals that include many crossings.

1.2.1 Metrics of Mixing

Two different (and generally unrelated) metrics should be used to describe chaotic advection in a bounded flow such as the one considered here: the size of the chaotic domain and the characteristic rate of mixing inside the chaotic domain.

The first of these two metrics is *the volume of the chaotic domain*, V_c. We define the volume and the dimensionality of mixing as the properties of the domain occupied (after a long time) by the tracers that originate in a small ball (say, size ε). For $\varepsilon = 0$, the whole interior is almost completely regular for any kind of perturbation. Actually, any

however minuscule perturbation (e.g., molecular diffusion) leads to 1D mixing: the dependence of $\Omega(i,j)$ in (1.2) on the values of I and/or J results in stretching of the original ball along $\Gamma_{i,j}$. This happens over order $O(1)$ times. In perturbed systems without singular surfaces, the tracers stay forever in the vicinity of the original surface of constant AI (see Figure 1.1a), eventually covering the whole surface $\Phi = \text{const}$. Thus we say that the adiabatic invariancy leads to 2D mixing.

In the presence of singular surfaces, a 3D chaotic domain of a finite size appears as soon as ε becomes nonzero. This is due to the fact that while the resonance phenomena are themselves local events (they are only affected by the dynamics in the vicinity of a corresponding surface), their effect is global, extending the chaotic domain to the scale of the entire flow. As a result, V_c depends on parameters of the base flow but not on the magnitude of perturbation, ε (for infinitesimal ε). Depending on parameters of the base flow (e.g., q in Section 1.3), the flow domain can be completely regular, partially regular and partially chaotic, or completely chaotic. The size of the chaotic domain is, to leading order, determined by the shape of its boundary – the torus τ_b tangential to the singular surface – which is independent of ε. However, for any finite ε, the boundary between the two domains is more complex. The chaotic domain penetrates inside τ_b adding a small layer (most often with thickness of order $\sqrt{\varepsilon}$, see [50] and Section 1.4 below for details). Further, small islands of stability may appear inside the mixing domain. As a result there are small corrections to V_c.

The second metric, the rate of mixing D, on the other hand, strongly depends on ε. Assuming statistical independence of consecutive crossings (see below), we can describe the evolution of the AI by a random walk with a characteristic step size of order ε^α, $0 < \alpha < 1$. Hence, after N crossings, the value of the AI changes by a quantity of the order $\sqrt{N} \times \varepsilon^\alpha$. The mixing can be considered complete when a typical chaotic streamline samples the entire chaotic domain. The difference between the values of the AI that bound the chaotic domain in our problem is of order unity. Therefore, it takes on the order of $N \sim \varepsilon^{-2\alpha}$ separatrix crossings for diffusion to cover the whole domain. As the typical time between successive crossings is of the order $1/\varepsilon$, we find the characteristic time for mixing to be $T_M = O(\varepsilon^{-1-2\alpha})$. This characteristic time diverges for $\varepsilon \to 0$, so the rate of mixing, defined as $D = 1/T_M = O(\varepsilon^{1+2\alpha})$, vanishes for $\varepsilon \to 0$.

For infinitesimal ε, the consecutive jumps can be considered statistically independent for most of the streamlines, so the accumulation of jumps can be described as a random walk *without* memory, leading to the standard Fokker–Planck equation for the probability density function (PDF) of the AI

$$\partial_t P = -\partial_\Phi(U_A P) + \partial_\Phi(D_A \partial_\Phi P) \tag{1.6}$$

where $P(\Phi, t)d\Phi$ is defined as the probability that at time t the tracer resides between the surfaces Φ and $\Phi + d\Phi$. The drift velocity U_A and the diffusion coefficient D_A are determined by the first and the second moments of the distribution of the jumps, respectively [51]. Since the jump magnitude distribution is a function of Φ, so are its moments. Moreover, since the dynamics between the jumps takes place on the

surfaces of constant AI, the time between the jumps is also a function of Φ [43]. Therefore, both $U_A(\Phi)$ and $D_A(\Phi)$ should be computed by taking this dependence into account.

1.2.2
Correlations of Successive Jumps and Ergodicity

Quantitative properties of the diffusion of the AI, in particular the validity of (1.6), depend on whether consecutive crossings are statistically dependent or independent. In volume-preserving systems, statistical independence (and, thus, the hypothesis of ergodicity, at least up to a residual of a small measure) for vanishing value of ε can be deduced from the divergence of resonance phases (denoted by ξ in the following sections) along streamlines. A similar problem for the Hamiltonian system was discussed in [10, 52, 53]. For finite values of ε the consecutive jumps become somewhat correlated, especially near the boundaries of the system. We discuss this in more details in Section 1.3.

Consider statistical properties of the jumps in Φ along one-phase trajectory of the system. Let two successive separatrix crossings be characterized by values ξ_1 and ξ_2. A small variation $\delta\xi_1$ in ξ_1 produces a variation of the jump in Φ by $\sim \varepsilon^{\alpha}\delta\xi_1$. In the period of time $\sim \varepsilon^{-1}$ before the next crossing, the value ξ_2 obtains a variation $\delta\xi_2 \sim \varepsilon^{\alpha-1}\delta\xi_1$. Thus $\delta\xi_2/\delta\xi_1 \sim \varepsilon^{\alpha-1} \gg 1$. Therefore, it is natural to suppose that ξ_1 and ξ_2 are statistically independent and the successive jumps in Φ are not correlated.

For many flows, it was verified numerically that inside the chaotic domain one does indeed find a positive Lyapunov exponent for $\varepsilon > 0$, confirming the divergence of nearby streamlines. Furthermore, for small ε, the flow possesses good ergodic properties inside the mixing domain, as the Poincaré sections illustrate, indicating very thorough mixing. Indeed, the chaotic domain is essentially devoid of regular islands, so a single streamline densely fills the whole chaotic domain. For decreasing ε, the regular islands (of size $\sqrt{\varepsilon}$) are expected to gradually disappear, resulting in perfect mixing.

1.3
Separatrix Crossings in Volume-Preserving Systems

In this section, we consider a flow where the presence of separatrix crossings results in the destruction of adiabatic invariance to illustrate different aspects of the evolution. The following problem was studied in details in [43].

Consider a microdroplet suspended at the free surface of a liquid substrate and driven using the thermocapillary effect with a constant speed in a straight line along the substrate surface [3, 54]. Experiments found the mixing to be very poor in this regime [54]. However, a numerical study of the simplified model of the flow constructed in [3] shows that the mixing efficiency can be improved dramatically by appropriately choosing the parameters such as the magnitude of the temperature coefficients of surface tension at different fluid interfaces, the ratio $\lambda = \mu_{\text{in}}/\mu_{\text{out}}$ of

the fluid viscosities inside and outside the droplet, and the curvature of the temperature field driving the flow.

To simplify the mathematical description of the problem, we follow [3, 43] assuming that the droplet is suspended below the free surface of the liquid substrate and consider the limit of small capillary numbers such that the droplet can be considered spherical. Under these assumptions, in nondimensional units (with distances scaled by the droplet radius and the origin located at the center of the drop), there are three component flows: the dipole flow $\mathbf{v}_d$

$$\begin{aligned} \dot{x}_d &= 1 + x^2 - 2r^2 \\ \dot{y}_d &= xy \\ \dot{z}_d &= xz \end{aligned} \tag{1.7}$$

the quadrupole flow $\mathbf{v}_q$

$$\begin{aligned} \dot{x}_q &= 2x(1 + x^2 - 2r^2) \\ \dot{y}_q &= y(r^2 + 2x^2 - 1) \\ \dot{z}_q &= z(r^2 + 2x^2 - 1) \end{aligned} \tag{1.8}$$

and the Taylor flow $\mathbf{v}_t$

$$\begin{aligned} \dot{x}_t &= z(\beta(5r^2 - 3 - 4x^2) + 2) \\ \dot{y}_t &= -4\beta xyz \\ \dot{z}_t &= x(\beta(5r^2 - 3 - 4z^2) - 2) \end{aligned} \tag{1.9}$$

where $r^2 = x^2 + y^2 + z^2$, $\beta = 1/(1+\lambda)$ (the value $\beta = 0.5$ is used in all numerical calculations), the x axis points in the direction of the thermal gradient, and the z axis is vertical. The components $\mathbf{v}_d$ and $\mathbf{v}_q$ are caused by the thermocapillary effect at the droplet surface, while $\mathbf{v}_t$ arises due to the thermocapillary effect at the surface of the liquid substrate. The complete flow inside the droplet can be written as a linear superposition of the dipole, Taylor, and quadrupole flows

$$\mathbf{v} = \mathbf{v}_d + \varepsilon \mathbf{v}_t + q\mathbf{v}_q \tag{1.10}$$

The parameters ε and q determine the relative strengths of the three components which depend on the temperature coefficients of surface tension at the droplet surface and the free surface of the substrate fluid and on the nonuniformity of the imposed temperature gradient [3]. As the dipole component is present in almost any setting, it is convenient to set its magnitude to unity by an appropriate choice of the timescale. In what follows, we will restrict our attention to the case of $|q| = O(1)$ and $0 \leq \varepsilon \ll 1$. This will allow us to describe the mixing process quantitatively using perturbation theory [8].

Flows (1.7)–(1.10) are volume preserving and bounded by the droplet surface $r = 1$, which represents an invariant set. Moreover, the plane $y = 0$ is an invariant set for each flow. Since the flow for $y < 0$ is a mirror image of the flow for $y > 0$ and there is no transport across the $y = 0$ plane, we will restrict our attention to the flow inside the hemisphere characterized by positive values of y.

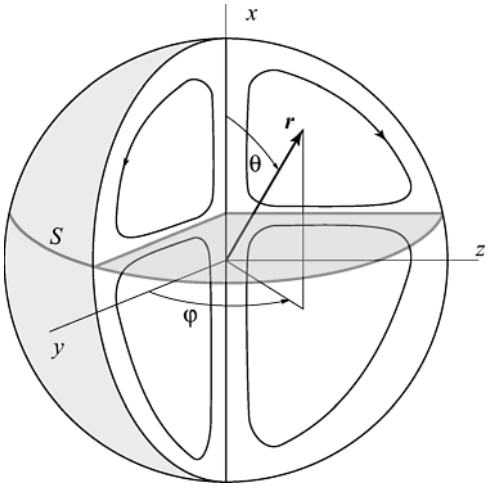

Figure 1.2 A sketch of the unperturbed flow for $|q| > 0.5$.

For $\varepsilon = 0$, flow (1.10) reduces to a superposition of the dipole and quadrupole flows and possesses two invariants: the azimuthal angle φ (around the x axis) and the streamfunction ψ:

$$\varphi = \arctan(z/y), \quad \psi = \frac{1}{2}(1+2qx)\varrho^2\left(1-r^2\right)$$

where we have defined $\varrho^2 = y^2 + z^2$. The flow structure of the unperturbed system depends on the value of q. Note that the dynamics for $q > 0$ is the same as for $q < 0$ up to the reflection with respect to the plane $x = 0$. There is always a pair of hyperbolic fixed points at the poles $x = \pm 1$, $\varrho = 0$ and, for $|q| > 0.5$, two circles of degenerate elliptic fixed points, accompanied by a hyperbolic fixed point $x = x_s \equiv -1/(2q)$, $\varrho = 0$ and a circle of degenerate hyperbolic fixed points on the surface at $x = x_s$, $r = 1$. The plane $x = x_s$ (denoted S below) is a separatrix (see Figure 1.2). Away from the separatrix, the axis, and the surface of the sphere, each joint level of the two integrals φ and ψ defines a closed unperturbed phase trajectory $\Gamma_{\varphi,\psi}$. The motion on $\Gamma_{\varphi,\psi}$ is periodic with frequency $\Omega(\psi)$. Note that if the base flow possesses axial symmetry, its frequency is naturally independent on azimuthal angle.

1.3.1 Flow Structure

For $\varepsilon \neq 0$, system (1.10) is no longer integrable. Integrals ψ and φ are not preserved. Streamlines are not closed and cross the separatrix S. Figure 1.3a represents a result of long integration of one perturbed-phase trajectory.

The structure of the phase portrait on the slow (φ, ψ) plane depends on the values of q. For $|q| < 0.5$, there is no separatrix, so the averaging procedure is valid everywhere and hence the AI is constant, if one ignores small bounded oscillations

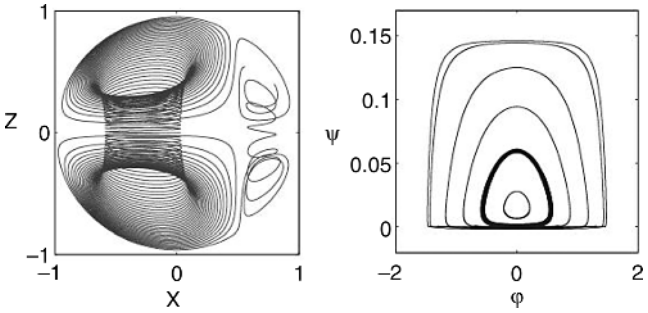

Figure 1.3 Dynamics of the perturbed system over one long period. The parameters are $q = -0.7$ and $= 10^{-2}$. (a) A perturbed streamline. (b) Phase portrait of the averaged system. The thick line in (b) shows the boundary of chaotic domain, l_b.

with amplitude of order ε. Therefore, the entire drop is a regular domain: all streamlines reside on the tori that are levels sets of the AI.

For $|q| > 0.5$, the separatrix plane defined by $x = x_s = -1/(2q)$ in the physical space (or $\psi = 0$ in the slow plane) appears inside the drop. For $0.5 < |q| < q_b$, the interior of the drop is divided between the regular domain and the chaotic domain. Numerically, we find $q_b \approx 0.96$. The regular domain corresponds to streamlines lying on the level sets of Φ that do not cross the separatrix (see Figure 1.3b), whereas the rest of the streamlines belong to the chaotic domain. To the leading order in ε, the boundary between the regular and the chaotic domain is a torus τ_b tangential to S. On the (φ, ψ) plane, τ_b corresponds to a closed curve l_b passing through the origin (see Figure 1.3b). Thus, we conclude that it is the level set $\Phi = \Phi(0,0)$ of the AI that serves as the boundary between the regular and the chaotic domains. Note that the level set $\Phi = \Phi(0,0)$ is not a sharp boundary: for any finite ε there are (although very few) regular trajectories inside the chaotic domain and vice versa. We will return to the discussion of the boundary between the domains in Section 1.4.

1.3.2
Dynamics Near the Separatrix Surface

For streamlines that cross the separatrix, the value of Φ may change significantly. It is shown in [43] that the jump of AI during a single passage of the exact system through the vicinity of S is

$$\Delta\overline{\Phi} = \sqrt{\varepsilon}\,\overline{\Phi}\left(1-\overline{\Phi}^2\right)^{1/4} f(\xi) \tag{1.11}$$

where $f(\xi)$ describes the dependence of the jump magnitude on the distance between the crossing point and the axis, parameterized by variable ξ, $\overline{\Phi} = \Phi/\Phi(0,0)$ is the normalized value of the AI. We refer the reader to [43] for the explicit definitions of $\xi, f(\xi)$, and $\Phi(0,0)$. The values of ξ and $\overline{\Phi}$ (and hence $\Delta\overline{\Phi}$) can be calculated exactly for any initial condition. However, a small change of order ε in the initial conditions produces, in general, a large (order 1) change in ξ. Hence, for

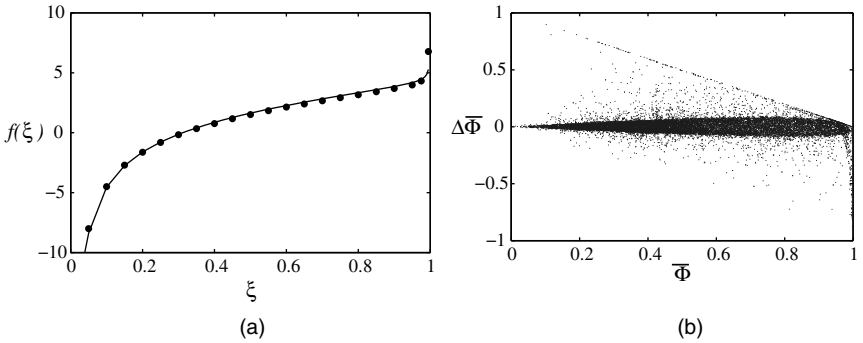

Figure 1.4 Jumps of AI: (a) the plot of $f(\xi)$. The solid line was obtained using analytical result (1.11) and the dots show the values obtained numerically from (1.10) for $\beta = 0.5$, $q = -1$, $= 10^{-3}$. (b) The distribution of the sizes of the jumps $\Delta\overline{\Phi}$ versus the values of $\overline{\Phi}$ before the crossings.

small ε it is possible to treat ξ as a random variable uniformly distributed on the unit interval [10].

Equation (1.11) was verified numerically for various values of parameters β, q, and ε. A typical plot of $f(\xi)$ is presented in Figure 1.4a. The function $f(\xi)$ – and hence $\Delta\overline{\Phi}$ – has singularities at both $\xi = 0$ and $\xi = 1$. Thus, there is a possibility (albeit quite small) of large changes in $\overline{\Phi}$ associated with a separatrix crossing. By direct calculation, the ensemble average of $\Delta\overline{\Phi}$ can be shown to vanish regardless of the value of $\overline{\Phi}$:

$$\langle \Delta\overline{\Phi} \rangle = \int_0^1 \Delta\overline{\Phi}(\xi, \overline{\Phi}) d\xi = 0 \tag{1.12}$$

1.3.3
Finite Perturbations

In most of the studies of resonance-induced chaotic diffusion, only infinitesimal perturbations were considered. To the best of our knowledge, the only papers that address, in any significant detail, the case of finite ε are [43, 53]. However, the dynamics in the presence of small but finite perturbations differs in several important ways from that with an infinitesimally small perturbation.

First, the very applicability of the method of averaging for larger ε is somewhat questionable as the ratio of the characteristic frequencies (e.g., $\Omega(\psi)$ and ε) may not be very large. Numerical simulations, however, indicate that the main result of the averaging method, that $\overline{\Phi}$ changes most significantly near the separatrix, holds for a wide range of ε. Moreover, this problem can be somewhat addressed by implementing the *improved adiabatic invariants*, see Section 1.4 below.

The second effect is that for finite values of ε, there is a finite probability that the jump size can become comparable to the range of the AI. Consequently, the

boundaries of the system start playing an important role in the statistics of the jumps. While magnitudes of most of the jumps are still given by (1.11) and satisfy the zero-average statement, the distribution of large jumps differs from the original prediction. Indeed, (1.11) breaks down when the value of $\overline{\Phi}$ either before or after the separatrix crossing is close to one of the domain boundaries. Take, for example, $\varepsilon = 10^{-3}$ and $q = -1$. Then, approximately 0.1% of the jumps feel the presence of the boundaries. While the influence of the boundaries on the properties and statistics of single crossings (albeit for a different system) was discussed in details in [53], here we are interested in necessary modifications to the long-time dynamics of the system and, in particular, the rate of mixing.

Figure 1.4b presents the distribution of the sizes of the jumps $\Delta\overline{\Phi}$ versus the values of $\overline{\Phi}$ before the corresponding crossing. There are three types of jumps. Most of the jumps are small and concentrate near the $\overline{\Phi}$ axis (the densely covered region). These jumps are well described by (1.11). In particular, the average value of these jumps is zero. The second type are jumps corresponding to points that lie between the lines $\overline{\Phi}_{n+1} = \overline{\Phi}_n + \Delta\overline{\Phi}_n = \pm 1$, but outside of the densely covered region. These jumps happen when streamlines pass through the vicinities of the singularities of $\Delta\overline{\Phi}(\xi)$, given by (1.11). Such jumps were studied in detail in [53]. Finally, there are jumps that lie on either of the lines $\overline{\Phi}_{n+1} = \overline{\Phi}_n + \Delta\overline{\Phi}_n = 1$ and $\overline{\Phi}_n = 1$. They were called "axis crossings" in [55].

1.4
Passages Through Resonances in Autonomous Flows

In the current section, we will discuss another type of phenomena that occur at singular surfaces: scattering on and capture into resonance in 3D autonomous flows of the action–action–angle type. As an example, we consider a volume-preserving kinematic model inspired by a Stokes Taylor–Couette flow between two infinite counter-rotating coaxial cylinders (the "vertical" z axis is along the axis of the cylinders, ϱ is the distance from the axis, and θ is an angle in the "horizontal" plane, see [14] for a complete description). In the dimensionless units, the flow is

$$\begin{aligned} \dot{\varrho} &= \varepsilon\kappa(\varrho-1)\cos\theta \\ \dot{z} &= \varepsilon(1+\ln\varrho/\ln\eta) \\ \dot{\theta} &= \omega(\varrho,z)-\frac{1}{\varrho}\varepsilon\kappa(2\varrho-1)\sin\theta \end{aligned} \tag{1.13}$$

The value of ϱ changes between $\varrho = 1$ (at the inner cylinder) and $\varrho = 1/\eta$ (at the outer cylinder). The frequency of the unperturbed flow, $\omega(\varrho, z)$, is

$$\omega(\varrho,z) = -\varrho\frac{\eta}{1-\eta} + \frac{1}{\varrho}\frac{1}{1-\eta} + \frac{\eta}{1-\eta^2}\delta\sin(\lambda z)\left(\varrho-\frac{1}{\varrho}\right) \tag{1.14}$$

where $\lambda = 2\pi$ and δ are the wavenumber and amplitude of oscillations of the frequency of the outer cylinder, respectively. One can see that $\omega = 1$ and

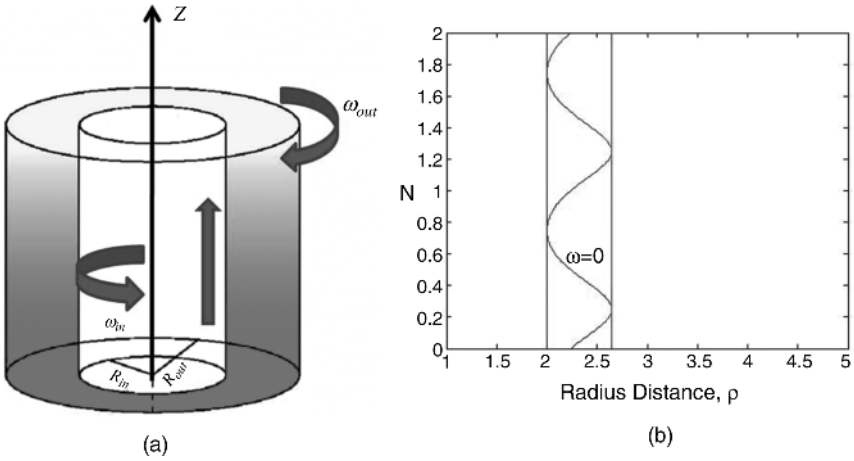

Figure 1.5 (a) The flow structure. (b) Division of the flow domain for z mod 1. A chaotic domain is between the vertical lines. A regular (KAM) domain consists of two parts at the left and at the right. The wavy line in the middle is the resonance, $\delta = 0.4$, $\eta = 0.2$.

$\omega = -1 + \delta \sin(\lambda z)$ on the inner and the outer cylinders, respectively. One can imagine the outer cylinder to consist of rings, each of which rotates with its own speed (see Figure 1.5a). The variables ϱ and z are the integrals of the unperturbed system. The unperturbed streamlines are circles with the direction of the rotation depending on the sign of $\omega(\varrho, z)$.

The perturbation consists of two parts. The first is a vertical (in the axial direction) shear-type flow (the $\dot{z}$ term). The second is an additional angular rotation due to a slight noncircularity of the outer cylinder. In (1.13), $0 \leq \varepsilon \ll 1$ is a small parameter, while $\kappa \sim 1$ defines a characteristic ratio of the two perturbations. The axial velocity, $\dot{z}$, equals ε at $\varrho = 1$ and vanishes at $\varrho = 1/\eta$.

For $\varepsilon > 0$, the variable θ is fast and the variables ϱ and z are slow. Thus, we can average (1.13) over one period of θ. The averaged trajectories (in the full 3D, (ϱ, z, θ), space) spiral around the cylinders of constant radius ($\varrho = \text{const}$) with the direction of the rotation depending on the sign of ω. The quantity

$$\Phi = \varrho$$

is an integral of the averaged system and is an AI of the exact system. The averaging is valid away from a resonance surface (in 3D), or a curve on the slow, (ϱ, z)-plane where $\omega = 0$. We denote that surface by R. It follows from (1.14) that R is given by

$$\varrho_R^2(z) = \frac{1}{\eta} \frac{1 + \eta - \eta\delta \sin(\lambda z)}{1 + \eta - \delta \sin(\lambda z)}$$

and located between $\varrho_{\min}$ and $\varrho_{\max}$. The division of the flow domain is shown in Figure 1.5b (note that we plotted z mod 1). Trajectories to the left and to the right of the corresponding vertical lines do not cross R.

As a passive tracer approaches R, it can be either *scattered at a resonance* or *captured into resonance*. While the scattering on resonance is somewhat similar to what happens at the separatrix crossing, capture can occur only at a resonance. Qualitatively, the difference between the two regimes can be described as follows. In the case of capture, upon arrival into the resonant zone, the phase switches its behavior from rotation to oscillation. The system drifts along the resonant surface for a long, of order ε^{-1}, time. As a result, the value of the AI changes by $\Delta\Phi = O(1)$. Among all the streamlines that arrive to the resonant zone during a given time interval (of order ε^{-1}), only a small, $O(\sqrt{\varepsilon})$ part of streamlines are captured. In the case of scattering there is no phase oscillation. The streamlines pass through the resonance zone in an $O(\sqrt{\varepsilon})$ time and the corresponding jump in the AI is $\Delta\Phi = O(\sqrt{\varepsilon})$. We describe these two processes below.

1.4.1 Scattering on Resonance

For most initial conditions, a tracer passes through the vicinity of R in a relatively short time and without capture. In such a case, in the first approximation we can fix the value of slow variables ω and z at the resonance values, and the dynamics is defined in terms of a forced-pendulum type of the second-order ODE for θ:

$$\theta'' = a + b_1 \cos\theta \tag{1.15}$$

where

$$a = \frac{\eta}{1-\eta^2}\delta\lambda\cos(\lambda z)\left(\varrho - \frac{1}{\varrho}\right)(1+\ln\varrho/\ln\eta) \quad b_1 = -2\kappa\frac{1}{\varrho+1}$$

and the prime denotes the derivative with respect to the rescaled time $\bar{t} = \sqrt{\varepsilon}\,t$. System (1.15) can be described by the resonance potential $V = -a\theta - b_1\sin\theta$. The shape of phase portraits for the motion in the potential V depends on the relation between a and b_1. If

$$|b_1| > |a| \tag{1.16}$$

the phase portrait looks like the one shown in Figure 1.6a, and vice versa for Figure 1.6b.

In the process of scattering, the value of Φ undergoes a jump, the magnitude of which is (in the main approximation) given by

$$\Delta\Phi = -2s\sqrt{\varepsilon}\kappa\frac{\varrho-1}{\sqrt{|a|}}\int_{s\infty}^{\bar{\theta}_*}\cos\theta\sqrt{2|s2\pi\xi + \theta + (b_1/a)\sin\theta|}\,\mathrm{d}\theta \tag{1.17}$$

where $\bar{\theta}_*$ is the value of θ at the crossing, $s = \mathrm{sign}\,(a)$, and $\xi = \{V(\theta_*)/(2\pi|a|)\} \in (0,1)$, where the curly brackets denote the fractional part. If (1.16) holds, the ensemble average of $\Delta\Phi$ is

$$\langle\Delta\Phi\rangle = -s\sqrt{\varepsilon}\frac{\varrho^2-1}{2\pi}S_R$$

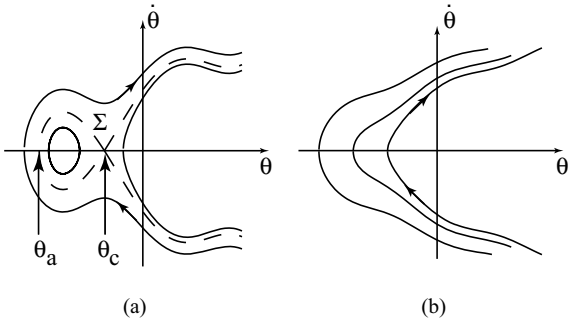

Figure 1.6 Schematic phase portraits on the (θ,θ) plane.

Here S_R is the area under the separatrix loop, Σ, in Figure 1.6a:

$$S_R = 2\left|\int_{\theta_a}^{\theta_c} \sqrt{-2(V-V_c)}\,\mathrm{d}\theta\right|$$

where V_c is the value of V at the hyperbolic fixed point in Figure 1.6a. If (1.16) does not hold, $\langle \Delta\Phi \rangle = 0$, as there is no separatrix, $S_R = 0$.

Equation (1.17) was checked numerically for various values of parameters ξ, κ, and ε. In Figure 1.7, the plots of $\Delta\varrho(\xi)/\sqrt{\varepsilon}$ are presented for (a) $\kappa = 2$ (when (1.16) is satisfied) and (b) $\kappa = 0.2$ (when (1.16) is not satisfied). The solid lines in Figure 1.7 correspond to theoretical values of $\Delta\varrho(\varepsilon)/\sqrt{\varepsilon}$ and the asterisks show values obtained numerically from (1.13) for various values of ξ. When (1.16) is satisfied, $\Delta\varrho(\xi)$ has a singularity.

1.4.2
Capture Into Resonance

The other phenomenon that affects the behavior of streamlines at a resonance crossing is capture into resonance. See [14, 56] for additional details. Capture is possible only if the phase portrait in the $(\theta, \dot{\theta})$-plane looks like the one shown in

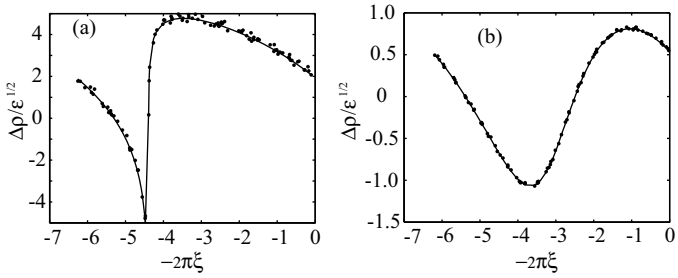

Figure 1.7 The plot of $\Delta\varrho/\sqrt{\varepsilon}$ as a function of ξ; (a) $\kappa = 2$ and (b) $\kappa = 0.2$. Note the difference in scales.

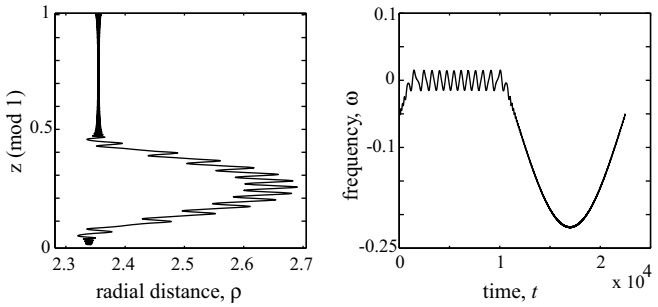

Figure 1.8 Captured motion. (a) A projection of a streamline on the slow, (ϱ, z), plane; and (b) the time evolution of $\omega(\varrho, z)$, $\varepsilon = 10^{-4}$, κ=2.

Figure 1.6a, in other words, if there is a separatrix in the $(\theta, \dot{\theta})$-plane. Let $\Pi(\varrho_*, z_*)$ be a flux of resonance flow through the separatrix loop in Figure 1.6a. The value of $\Pi(\varrho_*, z_*)$ changes as a phase point moves along a streamline. If $\Pi(\varrho_*, z_*)$ is decreasing, the capture is not possible. If Π increases and a streamline comes very close to the hyperbolic fixed point, it may cross Σ and, as a result, be caught in the oscillatory domain within the separatrix loop. In this case, a streamline starts shadowing the resonant surface. The captured motion is integrable and Hamiltonian. Depending on the structure of resonance, a tracer can be released from resonance (which is the case in the system under consideration) or reach the boundary of the system.

The dynamics of a typical capture is shown in Figure 1.8 as a projection on the slow, (ϱ, z), plane and the time evolution of $\omega(\varrho, z)$. A streamline comes from the bottom in Figure 1.8a (from the left in Figure 1.8b), is captured near $z = 0.05$ ($t = 100$), moves along the resonance, is released from the resonance near $z = 0.45$ ($t = 1000$), and then proceeds along an adiabatic path.

As it was discussed in [10, 13, 39], capture can be considered as a probabilistic phenomenon: initial conditions for streamlines that are or are not captured are mixed. The probability of capture for the streamlines starting inside a small ball centered at a certain point can be defined as a ration of the measure of the initial conditions that are captured to the full measure of the ball. It was proved in [10] that this probability is of the order of $O(\sqrt{\varepsilon})$.

1.4.3
Improved AI

As the value of ε increases, it becomes more and more difficult to distinguish between the jumps of AI in the process if scattering, which are of the order $O(\sqrt{\varepsilon})$ from oscillations of AI away from R, which are of the order $O(\varepsilon)$. In this situation the notion of *improved* AI becomes very useful. The improved AI $\Phi^{(1)}$ is given by

$$\Phi^{(1)} = \varrho - \varepsilon\kappa \frac{\varrho - 1}{\omega(z, \varrho)} \sin\theta$$

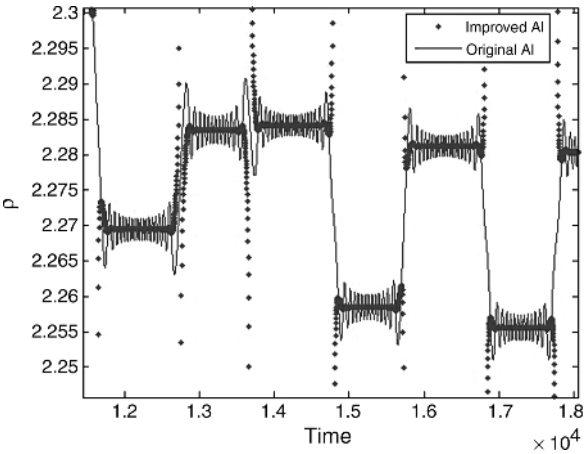

Figure 1.9 Comparison of improved AI with original AI (ϱ).

It can be checked by the direct calculations that oscillations of $\Phi^{(1)}$ away from the resonance are of the order of ε^2, while its jumps due to scattering or still $O(\sqrt{\varepsilon})$. However, there is no such a thing as free lunch: improved AI has a singularity at the resonance (which is natural as it contains ω in the denominator of the correction term), while the original AI remains finite, see Figure 1.9.

1.4.4
Jump of AI Between First- and Second-Layer Boundaries

The numerical simulations show that there is large transport of particles between the domain inside first-layer boundaries and the domain outside first-layer boundaries. We find out that the jump of the AI also happens for particles in the domain outside first-layer boundaries, where the resonance does not exist. The jump of AI happens at $z_{\text{in}} = 3/4$ and $z_{\text{out}} = 1/4$ (near the inner and outer first-layer boundary, respectively). Thus, the jump happens only once per slow period in the domain outside first-layer boundaries, instead of twice per slow period in the domain between first-layer boundaries.

The magnitude of $\Delta\varrho$ outside first-layer boundaries depends on both the value of θ at the point of closest approach and the distance between the particle and the first-layer boundary, shown in Figure 1.10a. When particles are close to the first-layer boundaries, the magnitude of $\Delta\varrho$ is large, and ω is relatively small (of order of $\sqrt{\varepsilon}$) at z_{in} close to the inner first-layer boundary, and at z_{out} close to the outer first-layer boundary. As particles move further from the first-layer boundaries, ω increases and the magnitude of $\Delta\varrho$ decreases. Figure 1.10b represents the variance of the distribution of $\Delta\varrho$ for uniformly distributed θ as the function of ϱ. The absolute values of $\Delta\varrho$ and the variance of the distribution of $\Delta\varrho$ decrease as the distance between particles and the first-layer boundaries increases. We can use the variance of $\Delta\varrho$ to estimate the approximate position of the boundaries which the streamlines that

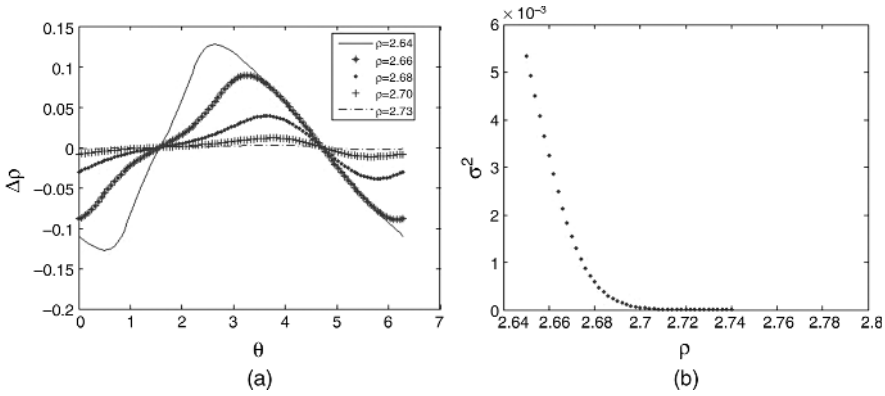

Figure 1.10 (a) The plot of $\Delta\varrho$ as a function of v for different values of ϱ. (b) The variance of distribution of $\Delta\varrho$ as a function of ϱ.

start in the mixing domain do not penetrate. The second-layer boundaries are the last invariant tori, and they are the actual boundaries of the chaotic domain.

1.4.5
Long-Time Dynamics and Adiabatic Diffusion

In many systems with random walks, the spreading of trajectories (or streamlines) can be described using diffusion-type equation(1.6). The coefficients, $U(\varrho)$ and $D(\varrho)$, are

$$U_A(\varrho) = \langle \Delta\varrho \rangle \quad D(\varrho) = \int_0^1 (\Delta\varrho(\xi) - \langle \Delta\varrho \rangle)^2 d\xi \tag{1.18}$$

As it was discussed above (and also illustrated below), for very small values of ε, U_A, averaged over a slow period, very often vanishes everywhere in the flow domain except in the very vicinity of the boundaries. The boundary conditions for solving diffusion equation (1.6) are von Neumann (no flux) at the outer boundary of the second-layer domain.

To study the validity of the adiabatic diffusion approximation, we performed a set of numerical simulations using the values of parameters specified above and $\varepsilon = 10^{-3}$, $\kappa = 0.2$. We choose 1000 initial uniformly distributed in a small cubic box in the size of ε picked from the middle of the chaotic domain. Its size was $\varrho_{\text{in}} \times z_{\text{in}} \times \theta_{\text{in}} = [2.220, 2.229] \times [0.251, 0.260] \times [0.011, 0, 020]$. We considered the Poincaré sections located at $z = N + 0.25$ and $z = N + 0.75$, where N is a set of integer numbers. Every trajectory crosses the resonance once between two consecutive sections.

The results of our numerical simulations showed that the particles which initially concentrated in those small boxes start to diffuse after multiple resonance crossings, and in the end, the distribution of particles in the radius direction is quite uniform, shown in Figure 1.11. The solid line in Figure 1.11 is the solution of diffusion

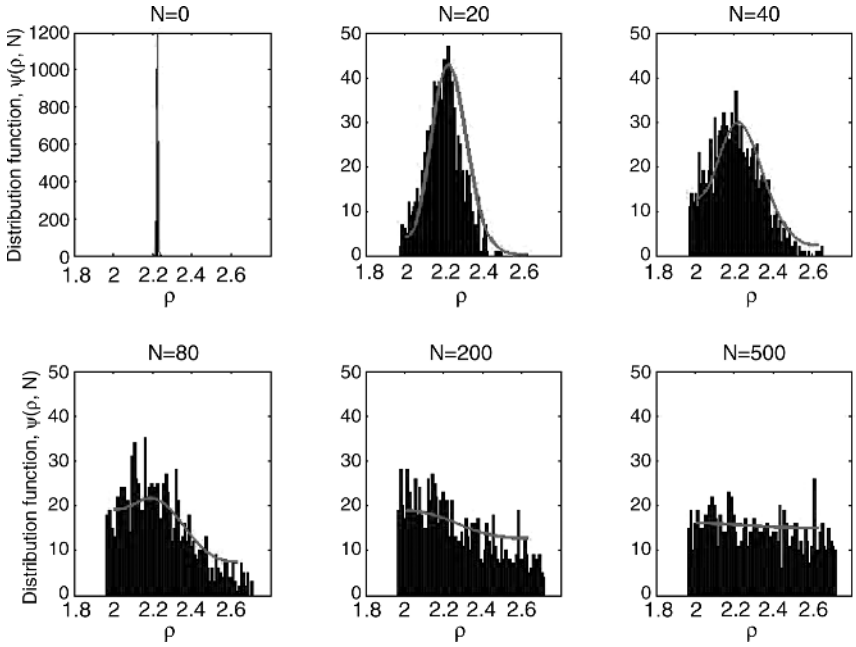

Figure 1.11 The histogram of $P(\varrho, N)$ after different numbers of resonance crossings for Box 1.

equation (1.6) using the said box as the initial condition, and both results are consistent with each other. The same results are also obtained for other initial conditions, located in different parts of the flow domain.

The second moment of the distribution function $P(\varrho, N)$ of numerical simulations, σ^2, is shown as the dash line in Figure 1.12. The constant slope of the solid line in Figure 1.12 is the diffusion coefficient $D(\varrho)$ analytically calculated using Eq. (1.18) for ($\langle \varrho_0 \rangle = 2.225$) (in the center of the box). The second moment of numerical simulations σ^2 is very close to $D(\varrho)$ in the beginning, before particles reaching the first-layer boundaries. However, when particles start to cross the first-layer boundaries, σ^2 and $D(\varrho)$ start to diverge. In the end, σ^2 comes to an asymptotic value with small oscillations. That asymptotic value is the variance of uniformly distributed particles in the chaotic domain, shown as horizontal lines in Figure 1.12.

1.5
Passages Through Resonances in Nonautonomous Flows

The effect of resonances is quite richer in the multifrequency systems. An example of such systems is nonautonomous flows, where the time appears explicitly as an additional fast phase. In the present section we follow [4] and discuss the mixing dynamics in such systems and, as an example, we consider an incompressible fluid flow in a one-dimensional array of cubic cells described by the following equations:

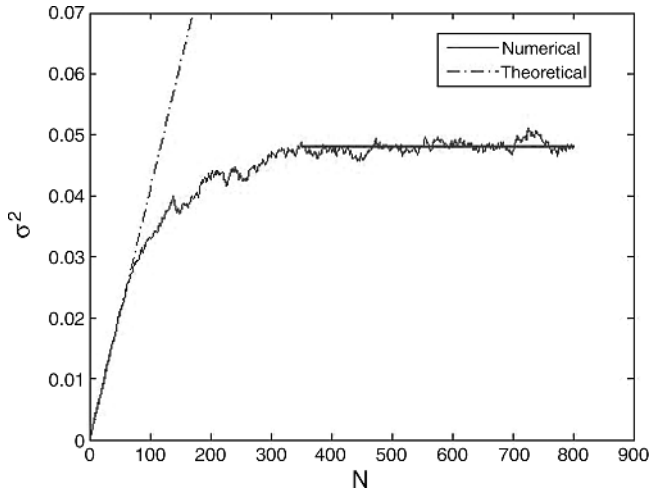

Figure 1.12 The variance of ϱ, over 1000 trajectories as a function of the number of resonance crossings for Box 1.

$$\begin{aligned}\dot{x} &= -\cos(\pi x)\sin(\pi y) + \pi b \sin(\pi x)\sin(\pi y)\sin\omega t \\ &+ \varepsilon \sin(2\pi x)\sin(\pi z) \\ \dot{y} &= \sin(\pi x)\cos(\pi y) + \pi b \cos(\pi x)\cos(\pi y)\sin\omega t \\ &+ \varepsilon \sin(2\pi y)\sin(\pi z) \\ \dot{z} &\quad 2\varepsilon\cos(\pi z)[\cos(2\pi x) + \cos(2\pi y)]\end{aligned} \tag{1.19}$$

This is a linearization of a system introduced by Solomon and Mezic in [57] as a qualitative model of a Lorenz-force driven cellular flow in a channel of rectangular cross-section ($-0.5 < y, z < 0.5$). It is easy to check that the no-slip boundary condition at the channel walls is not satisfied. However, the exact solution of the Navier–Stokes equations satisfying the proper boundary conditions will lead us to qualitatively the same conclusions while making the calculations unnecessarily complicated. The terms proportional to ε describe a weak correction to the main recirculation flow caused by inertial effects (Eckman pumping). The time dependence of the flow represents an external perturbation describing the shift, with amplitude b, of the boundaries between the cells (planes $x = n + 1/2$, $n \in Z$). For nonzero b, there is transport between the cells; however, our objective here is to understand the transport properties of the flow inside each of the cells. Since the dynamics in all the cells are identical, we will consider only the cell with $-0.5 < x < 0.5$.

1.5.1 Unperturbed Flow

First, consider the unperturbed (base) flow characterized by $\varepsilon = 0$ and $b = 0$. In this case, (1.19) is reduced to

$$\dot{x} = -\cos(\pi x)\sin(\pi y) \quad \dot{y} = \sin(\pi x)\cos(\pi y) \quad \dot{z} = 0 \tag{1.20}$$

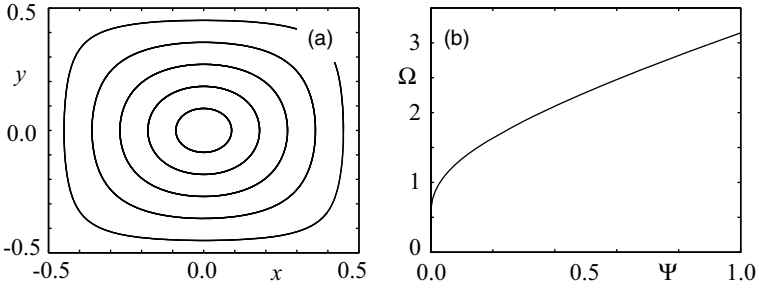

Figure 1.13 Unperturbed system: (a) typical streamlines in the $z = \text{const}$ plane and (b) the frequency $\Omega(\Psi)$.

This is a two-dimensional autonomous flow which possesses two invariants:

$$z = \text{const} \quad \Psi = \cos(\pi x)\cos(\pi y) = \text{const}$$

with Ψ proportional to the streamfunction of the unperturbed flow in the (x, y) plane. All the streamlines $\Gamma_{z,\Psi}$ of the unperturbed flow are closed (see Figure 1.13a) with the period of motion $T(\Psi)$. The corresponding frequency $\Omega = 2\pi/T$ ranges from $\Omega = 0$ at the boundaries of the cell to $\Omega = \pi$ in the center. On every $\Gamma_{z,\Psi}$, we can introduce a uniform phase χ mod (2π) such that $\chi = 0$ on the positive x-axis and $\dot{\chi} = \Omega(\Psi)$. Due to the dependence of Ω of Ψ, the unperturbed flow is characterized by mixing in only one dimension (along the streamlines $\Gamma_{z,\Psi}$) at $O(1)$ rate.

1.5.2
Two Perturbations and Averaging

Next, consider the effect of the Eckman pumping ($\varepsilon > 0$), ignoring the time-dependent shift for the moment ($b = 0$). In this limit, flow (1.19) is steady but conserves neither z nor Ψ. The dynamics is characterized by two different timescales: the variable χ is fast (changes on $O(1)$ timescale), while the variables z and Ψ are slow (change on $O(\varepsilon^{-1})$ timescale). Averaging evolution equations for $\dot{\Psi}$ and $\dot{z}$ over the quick oscillations in χ over one period of the unperturbed motion, we obtain an averaged system that possesses an AI Φ defined as a flux of the vector field $\mathbf{v}_\varepsilon$ (the ε-dependent part of the perturbation in (1.19), through a surface S_Γ bounded by an unperturbed streamline $\Gamma_{z,\Psi}$). The averaged system can be written as

$$\dot{\Psi} = -\varepsilon \frac{\pi}{T(\Psi)} \frac{\partial \Phi}{\partial z} \quad \dot{z} = \varepsilon \frac{\pi}{T(\Psi)} \frac{\partial \Phi}{\partial \Psi} \tag{1.21}$$

The addition of the time-dependent perturbation makes the structure of the flow much more complex if b and ε are of similar magnitude. Hence, in what follows we assume $\beta \equiv b/\varepsilon = O(1)$. Furthermore, we assume $\omega = O(\Omega) = O(1)$. The evolution equations for the slow variables are

$$\dot{\Psi} = -2\pi\varepsilon \sin(\pi z)\Psi\left(\sin^2(\pi x) + \sin^2(\pi\gamma)\right) - \varepsilon\frac{\pi^2}{2}\beta(\sin(2\pi\gamma)\sin(\omega t))$$
$$\dot{z} = 2\varepsilon \cos(\pi z)[\cos(2\pi x) + \cos(2\pi\gamma)] \tag{1.22}$$

If Ω and ω are incommensurate, then averaging over χ and t can be performed independently (see, e.g., [58]). In this case, the time-dependent terms in the equation for $\dot{\Psi}$ average out and we would expect the AI Φ to be conserved as before. The evolution over a longer time interval shows that the AI remains essentially constant except for the short periods of time when $\Omega \approx \omega$, as Figure 1.14b illustrates. We therefore find, as previous studies [7, 59–61] did, a clear indication of the fact that the breakdown of adiabatic invariance is a consequence of processes occurring in the vicinity of resonances.

1.5.3
Resonant Phenomena

As the value of Ψ slowly drifts, so does $\Omega(\Psi)$. Hence, at certain values of Ψ a resonance condition

$$n\Omega(\Psi) - \omega = 0 \tag{1.23}$$

is satisfied for some nonzero integer n. Note that (1.23) is a special case of a more general resonance condition $n\Omega = m\omega$, which corresponds to a generic time-periodic perturbation. The restriction to $m = 1$ in our case is a consequence of the particular form of the time-dependent perturbation in (1.19), namely, that only the first harmonic is present. Since Ω is independent of z, all resonance surfaces R_n, defined by $\Psi(x, y) = \Psi_n \equiv \Omega^{-1}(\omega/n)$, are vertical cylinders in the physical space or vertical lines $\Psi = \Psi_n$ in the slow plane (see Figure 1.14b).

In what follows we describe a quantitative description of the dynamics near resonant surfaces based on the theory of resonance phenomena in multiple-frequency systems [58]. Note that, unlike autonomous systems with resonance phenomena (see, e.g., [14], and Section 1.4) where the fast (unperturbed) dynamics slows

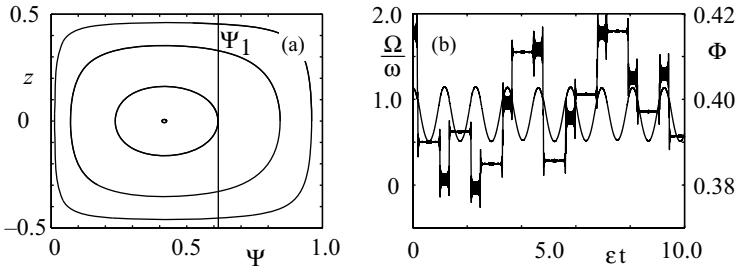

Figure 1.14 The complete flow with $\varepsilon = b = 10^{-4}$ and $\omega = 2.5$: (a) projection of the averaged system on the slow plane, the bold line is the 1 : 1 resonance is shown; (b) plots of Ω/ω (dashed line) and Φ (solid line) versus time for complete flow (1.1).

down near a resonance, for the flow studied here, near R_n both the fast angle variable χ and the phase of the perturbation ωt keep changing rapidly. It is only a particular linear combination of these phases that slows down:

$$\gamma = n\chi - \omega t \tag{1.24}$$

Therefore, near every resonance surface there is just one fast variable, χ, rather than two far from the resonances. Of the three other variables, Ω and z are slow and γ is semislow with characteristic rates of change of order $O(\varepsilon)$ and $O(\varepsilon^{1/2})$, respectively. We can still average the exact equations of motion for all three slow and semislow variables over χ (perform the so-called *partial averaging*, see [58]) in order to obtain equations of motion near a resonance surface:

$$\gamma' = \frac{1}{\sqrt{\varepsilon}}(n\Omega - \omega) \quad \Omega' = \sqrt{\varepsilon}\frac{\partial \Omega}{\partial \Psi}\frac{\dot{\Psi}}{\varepsilon} \quad z' = \sqrt{\varepsilon}\frac{\dot{z}}{\varepsilon} \tag{1.25}$$

In (1.25), the prime denotes the derivative with respect to the rescaled time $\bar{t} = \sqrt{\varepsilon}\, t$ and $\dot{\Psi}$, $\dot{z}$ were defined in (1.22). Equation (1.25) is very similar to the one appearing in autonomous case (see (1.15)).

For most initial conditions, tracers pass through the vicinity of resonance in a relatively short time and the value of Φ undergoes a relatively small jump. In the first approximation we can fix the value of slow variables Ω and z at the resonance values, which yields a forced pendulum-like equation for γ:

$$\gamma'' = \frac{1}{\sqrt{\varepsilon}} n\Omega' = a_n + b_n \cos\gamma \tag{1.26}$$

In (1.26), a_n and b_n correspond to the average of the first and the second term in (1.22) over the fast period $T_n \equiv T(\Psi_n) = 2\pi n/\omega$, respectively:

$$a_n = -n\Psi \sin(\pi z_*)\frac{\partial \Omega}{\partial \Psi}\int_0^{2\pi} \left(\sin^2(\pi x) + \sin^2(\pi\gamma)\right) \mathrm{d}\chi$$

$$b_n = -\frac{\pi}{4} n\beta \frac{\partial \Omega}{\partial \Psi}\int_0^{2\pi} \sin(2\pi\gamma)\sin(n\chi)\mathrm{d}\chi$$

and z_* is the value of z at which the crossing occurs. The average of $\dot{\Phi}$ over T_n can be computed using (1.21) and (1.22), yielding

$$\langle \dot{\Phi} \rangle = \varepsilon\pi\beta\, c_n \cos(\pi z_*)\cos\gamma \tag{1.27}$$

where the coefficient c_n is given by

$$c_n = -\frac{n}{\omega}\int_0^{2\pi} (\cos(2\pi x) + \cos(2\pi\gamma))\sin(2\pi\gamma)\sin(n\chi)\mathrm{d}\chi.$$

Integrating over a time interval during which the resonance is crossed once, we obtain in the leading order

$$\Delta\Phi = -2\sqrt{\varepsilon}\, s\, \pi\beta \cos(\pi z_*) \frac{c_n}{\sqrt{|a_n|}} \int_{-s\infty}^{\gamma(t_*)} \frac{\cos\gamma}{\sqrt{2|s2\pi\xi + \gamma + (b_n/a_n)\sin\gamma|}} \mathrm{d}\gamma$$

where ξ is defined analogously to the previous section.

When $|b_n| > |a_n|$, $\langle\Delta\Phi\rangle$ is finite:

$$\langle\Delta\Phi\rangle = -s\sqrt{\varepsilon}\,\beta \cos(\pi z_*) \frac{c_n}{b_n} S$$

where S is the area under the separatrix loop on the resonance plane (cf. Figure 1.6a). In the opposite case $|b_n| < |a_n|$, there is no separatrix, $S = 0$, and hence $\langle\Delta\Phi\rangle = 0$. Generally, a nonzero ensemble average of $\Delta\Phi$ results in a unidirectional drift of Φ. However, in the current problem, two successive crossings occur at almost the opposite values of z. Thus, they cancel each other *on average* because of the change of the sign of s, and the aggregate change of Φ on one period of the slow motion has zero mean. The second moment of $\Delta\Phi$

$$\sigma^2 = \int_0^1 (\Delta\Phi(\xi) - \langle\Delta\Phi\rangle)^2 \mathrm{d}\xi,$$

is finite for any value of Φ. The dependence of $\Delta\Phi$ on the order of the resonance is determined by the scaling of a_n, b_n, and c_n, which are the Fourier coefficients of smooth functions. In particular, a_n corresponds to the 0-th harmonic and increases linearly with n. On the other hand, b_n and c_n correspond to higher harmonics and decrease exponentially with n. As a consequence, the characteristic magnitude of the jumps decays exponentially. Thus, only low-order resonances contribute significantly to the change in the value of the AI. For high-order resonances, we have $\Delta\Phi \sim \sqrt{\varepsilon}\, e^{-\alpha n}$, where α is some constant.

1.5.4
Volume of the Mixing Domain

On every period $T_\varepsilon(\Phi)$ of the slow motion along a given trajectory, the value of Ψ changes between $\Psi_{\min}$ and $\Psi_{\max}$. If no (low-order) resonance Ψ_n falls in this interval, then that trajectory (and all trajectories inside of it) remains regular. If, on the other hand, the trajectory crosses a resonance surface, the AI experiences jumps and the motion becomes chaotic.

In the $\varepsilon \to 0$ limit, the boundary between the chaotic and the regular domains is, thus, given by the trajectory Γ_{Φ^*} that (i) touches a resonance surface and (ii) has the largest value Φ among all such trajectories on the (Ψ, z) plane (bold line in Figure 1.14a). Condition (ii) is necessary when multiple resonances are considered. In the physical space, the boundary is formed by the corresponding torus τ_{Φ^*}. The Poincaré section of the complete flow by the plane $z = 0$ (see Figure 1.15a) confirms that the space inside the torus τ_{Φ^*} corresponds to the regular domain discovered in [57], while the rest of the physical space belongs to the chaotic domain. Moving the frequency ω closer to the resonance with $\Omega(\Psi_c) \approx 2.2$ completely wipes out the regular domain (see Figure 1.15b).

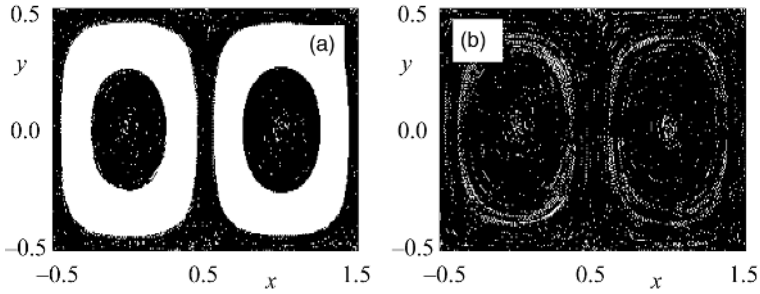

Figure 1.15 Complete and partial mixing. $z = 0$ Poincaré section of a single streamline with $\varepsilon = b = 10^{-4}$ and (a) $\omega = 4.0$, (b) $\omega = 2.5$.

The width d of the regular domain can be computed easily for any value of ω (see Figure 1.16). For $0 < \omega \ll 1$, all the resonances are located near $\Psi = 0$ (i.e., cell boundary). As ω is increased, the $1:1$ resonance is the first to penetrate deeper into the cell. For $0 < \omega\pi$, Γ_{Φ^*} is tangent to the resonance $\Psi = \Psi_1$ (see Figure 1.14a). As ω approaches π, the $1:1$ resonance is pushed out of the cell and the $1:3$ resonance becomes the most prominent for $\pi\omega 3\pi$ (recall that even resonances do not lead to jumps in Φ and thus do not contribute to adiabatic diffusion). Then the process repeats itself: as ω is increased further, low-order resonances are pushed out of the cell and higher resonances become prominent. Finally, as $\omega \to \infty$, the cell becomes uniformly covered by high-order resonances. However, the impact of the high resonances is exponentially small and hence we can expect mixing to become spatially uniform on exponentially long timescales. On finite timescales characteristic of experiments (e.g., those reported in [57]), it would appear that no mixing is taking place. We should also point out that, for the flow between concentric spheres considered in [60, 61], complete mixing relies on high-order resonances and, while conceptually possible, would similarly require exceedingly long times.

In our case, complete mixing on experimentally accessible timescales can be achieved by eliminating the domain of regular dynamics via a proper placement of a low-order resonance. This can be accomplished by setting the frequency ω of the

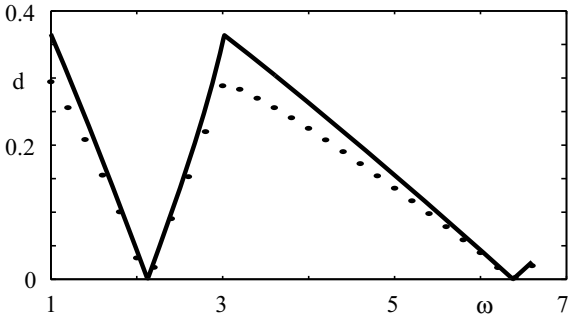

Figure 1.16 The width d of the regular domain as a function of the perturbation frequency, ω for $\varepsilon = b = 10^{-4}$: solid line – theoretical prediction, dots – numerical simulations.

perturbation such that $\Psi_n(\omega) = \Psi_c$ for some n. More precisely, the resonance must be within the interval $|\Psi_n - \Psi_c| = O(\sqrt{\varepsilon})$, as the chaotic domain penetrates inside Γ_{Φ^*} by an $O(\sqrt{\varepsilon})$ distance [50]. This property, negligible in most similar problems, is important here as the magnitude of the jumps vanishes at Ψ_c. Indeed, $\dot{\Phi} \sim \dot{z}$ according to (1.27), so $\Delta\Phi = 0$ at $\Psi = \Psi_c$, as $\dot{z} = 0$ there. Since the width of the regular domain $d \sim |\Psi_n(\omega) - \Psi_c|$, we find the width of the frequency intervals yielding complete mixing (where $d \approx 0$) to scale as $\Delta\omega \sim \sqrt{\varepsilon}$ (see Figure 1.16).

Acknowledgments

This work was supported in part by the National Science Foundation (project CBET-0900177) and the Russian Foundation for Basic Research (projects 09-01-00333, 08-02-00201). The author is grateful to his co-authors Roman Grigoriev, Igor Mezic, Anatoly Neishtadt, Alexei Vasiliev, and John Widloski.

References

1 Mezic, I. and Wiggins, S. (1994) On the integrability and perturbation of three-dimensional fluid flows with symmetry. *Journal of Nonlinear Science*, **4**, 157–194.
2 Haller, G. and Mezic, I. (1998) Reduction of three-dimensional, volume preserving flows by symmetry. *Nonlinearity*, **11**, 319.
3 Grigoriev, R.O. (2005) Chaotic mixing in thermocapillary-driven microdroplets. *Physics of Fluids*, **17**, 033601.
4 Vainchtein, D.L., Widloski, J., and Grigoriev, R.O. (2008) Resonant mixing in perturbed action–action–angle flow. *Physical Review E*, **78**, art: 026302.
5 Laskar, J. (1996) Large scale chaos and marginal stability in the solar system. *Celestial Mechanics & Dynamical Astronomy*, **64**, 115–162.
6 Dellnitz, M., Junge, O., Koon, W.S., Lekien, F., Lo, M.W., Marsden, J.E., Padberg, K., Preis, R., Ross, S.D., and Thiere, B. (2005) Transport in dynamical astronomy and multibody problems. *International Journal of Bifurcation and Chaos*, **15**, 699–727.
7 Feingold, M., Kadanoff, L.P., and Piro, O. (1988) Passive scalars, 3-dimensional volume-preserving maps, and chaos. *Journal of Statistical Physics*, **50**, 529–565.
8 Arnold, V.I., Kozlov, V.V., and Neishtadt, A.I. (1988) *Dynamical Systems III*. *Encyclopedia of Mathematical Sciences*, Springer, New York, NY.
9 Vainshtein, D.L., Vasiliev, A.A., and Neishtadt, A.I. (1996) Changes in the adiabatic invariant and streamline chaos in confined incompressible Stokes flow. *Chaos*, **6**, 67–77.
10 Neishtadt, A.I. (1999) On adiabatic invariance in two-frequency systems. in: Hamiltonian systems with 3 or more degrees of freedom. *NATO ASI Series C*, **533**, 193–213.
11 Chirikov, B.V. (1959) Passage of nonlinear oscillatory system through resonance. *Soviet Physics Doklady*, **4**, 390–394.
12 Kevorkian, J. (1974) Model for reentry roll resonance. *SIAM Journal on Applied Mathematics*, **26**, 638–669.
13 Neishtadt, A.I. (1997) Scattering by resonances. *Celestial Mechanics & Dynamical Astronomy*, **65**, 1–20.
14 Vainchtein, D.L., Neishtadt, A.I., and Mezic, I. (2006) On passage through resonances in volume-preserving systems. *Chaos*, **16**, 043123.
15 Neishtadt, A.I. (1986) Change of an adiabatic invariant at a separatrix. *Soviet Journal of Plasma Physics*, **12**, 568–573.
16 Cary, J.R., Escande, D.F., and Tennyson, J.L. (1986) Adiabatic-invariant change due

to separatrix crossing. *Physical Review A*, **34**, 4256–4275.

17 Haberman, R. and Bourland, F.J. (1994) Slow passage through homoclinic orbits for the unfolding of a saddle-center bifurcation and the change in adiabatic invariant. *Studies in Applied Mathematics*, **91**, 95–124.

18 Vainshtein, D.L., Zelenyi, L.M., Neishtadt, A.I., and Savenkov, B.V. (1999) Jumps in an adiabatic invariant with small initial values. *Plasma Physics Reports*, **25**, 333–337.

19 Diminnie, D.C. and Haberman, R. (2002) Connection across a separatrix with dissipation. *Physica D*, **162**, 34–52.

20 Neishtadt, A.I. and Vasiliev, A.A. (1999) Change of the adiabatic invariant at a separatrix in a volume-preserving 3D system. *Nonlinearity*, **12**, 303–320.

21 Ward, T. and Homsy, G.M. (2003) Electrohydrodynamically driven chaotic mixing in a translating drop. II. Experiments. *Physics of Fluids*, **15**, 2987–2994.

22 Grigoriev, R.O., Schatz, M.F., and Sharma, V. (2006) Chaotic mixing in microdroplets. *Lab Chip*, **6**, 1369–1372.

23 Paik, P., Pamula, V.K., Pollack, M.G., and Fair, R.B. (2003) Rapid droplet mixers for digital microfluidic systems. *Lab Chip*, **4**, 253–259.

24 Fowler, J., Moon, H., and Kim, C.-J. (2002) Enhancement of mixing by droplet-based microfluidics. in Proc. IEEE Conf. MEMS, pp. 97–100.

25 Song, H., Tice, J.D., and Ismagilov, R.F. (2003) A microfluidic system for controlling reaction networks in time. *Angewandte Chemie-International Edition*, **42**, 768–772.

26 Belbruno, E. and Marsden, B.G. (1997) Resonance hopping in comets. *Astronomical Journal*, **113**, 1433–1444.

27 Jaffe, C., Ross, S.D., Lo, M.W., Marsden, J., Farrelly, D., and Uzer, T. (2002) Statistical theory of asteroid escape rates. *Physical Review Letters*, **89**, 011101.

28 Neishtadt, A.I. and Sidorenko, V.V. (2004) Wisdom system: Dynamics in the adiabatic approximation. *Celestial Mechanics & Dynamical Astronomy*, **90**, 307–330.

29 Zabiego, M., Ghendrih, P., Becoulet, M., Costanzo, L., De Michelis, C., Friant, C., and Gunn, J. (2001) Characterisation of the separatrix position in the ergodic divertor discharges of the tore supra tokamak. *Journal of Nuclear Materials*, **290**, 985–989.

30 Lehnen, M. *et al.* (2005) Transport and divertor properties of the dynamic ergodic divertor. *Plasma Physics and Controlled Fusion*, **47**, B237–B248.

31 Jakubowski, M.W. *et al.* (2006) Change of the magnetic-field topology by an ergodic divertor and the effect on the plasma structure and transport. *Physical Review Letters*, **96**, 035004.

32 Gendelman, O., Manevitch, L.I., Vakakis, A.F., and M'Closkey, R. (2001) Energy pumping in nonlinear mechanical oscillators: Part I – Dynamics of the underlying Hamiltonian systems. *Journal of Applied Mechanics – Transactions of the ASME*, **68**, 34–41.

33 Vakakis, A.F. and Gendelman, O. (2001) Energy pumping in nonlinear mechanical oscillators: Part II – resonance capture. *Journal of Applied Mechanics-Transactions of the ASME*, **68**, 42–48.

34 Popov, A.A., Thompson, J.M.T., and McRobie, F.A. (2001) Chaotic energy exchange through auto-parametric resonance in cylindrical shells. *Journal of Sound and Vibration*, **248**, 395–411.

35 Itin, A.P., Neishtadt, A.I., and Vasiliev, A.A. (2001) Resonant phenomena in slowly perturbed rectangular billiards. *Physics Letters A*, **291**, 133–138.

36 Chernikov, A.A. and Schmidt, G. (1994) Adiabatic chaos in Josephson-junction arrays. *Physical Review E*, **50**, 3436–3445.

37 Vasiliev, A.A., Neishtadt, A.I., and Itin, A.P. (1997) On dynamics of four phase-coupled oscillators with close frequencies. *Regular and Chaotic Dynamics*, **3**, 1–9.

38 Ashour-Abdalla, M., Frank, L., Paterson, M., Peroomian, V., and Zelenyi, L.M. (1996) Proton velocity distributions in the magnetotail: Theory and observations. *Journal of Geophysical Research*, **101**, 2587–2598.

39 Itin, A.P., Neishtadt, A.I., and Vasiliev, A.A. (2000) Captures into resonance and scattering on resonance in dynamics of a charged relativistic particle in magnetic

field and electrostatic wave. *Physica D*, **141**, 281–296.

40 Vainchtein, D.L., Rovinsky, E.V., Zelenyi, L.M., and Neishtadt, A.I. (2004) Resonances and particle stochastization in nonhomogeneous electromagnetic fields. *Journal of Nonlinear Science*, **14**, 173–205.

41 Vainchtein, D.L., Vasiliev, A.A., and Neishtadt, A.I. (2009) Electron dynamics in a parabolic magnetic field in the presence of an electrostatic wave. *Plasma Physics Reports*, **35** (12), 1021–1031.

42 Neishtadt, A.I., Artemyev, A.V., Zelenyi, L.M., and Vainshtein, D.L. (2009) Surfatron acceleration in electromagnetic waves with a low phase velocity. *JETP Letters*, **89**, 441–447.

43 Vainchtein, D.L., Widloski, J., and Grigoriev, R.O. (2007) Mixing properties of steady flow in thermocapillary driven droplets. *Physics of Fluids*, 19:art, 067102.

44 Vainchtein, D.L., Widloski, J., and Grigoriev, R.O. (2007) Resonant chaotic mixing in a cellular flow. *Physical Review Letters*, 99:art, 094501.

45 Bogolyubov, N.N. and Mitropolsky, Yu.A. (1961) *Asymptotic Methods in the Theory of Nonlinear Oscillations*, vol. **537**, Gordon and Breach Science Publishers, New York.

46 Arnold, V.I. (1983) *Geometrical Methods in the Theory of Ordinary Differential Equations*, Springer, New York, Heidelberg, Berlin.

47 Timofeev, A.V. (1978) On the constancy of an adiabatic invariant when the nature of the motion changes. *Soviet Physics – JETP*, **48**, 656–659.

48 Neishtadt, A.I. (1987) On the change in the adiabatic invariant on crossing a separatrix in systems with two degrees of freedom. *PMM USSR*, **51**, 586–592.

49 Neishtadt, A.I., Vainshtein, D.L., and Vasiliev, A.A. (1998) Chaotic advection in a cubic Stokes flow. *Physica D*, **111**, 227–242.

50 Vainshtein, D.L., Vasiliev, A.A., and Neishtadt, A.I. (1996) Adiabatic chaos in a two-dimensional mapping. *Chaos*, **6**, 514–518.

51 Hughes, B.D. (1995) *Random Walks and Random Environments*, Oxford University Press, New York.

52 Dolgopyat, D. (2004) Repulsion from resonances. Preprint of U. Maryland.

53 Neishtadt, A.I., Simo, C., and Vasiliev, A.A. (2003) Geometric and statistical properties induced by separatrix crossings in volume-preserving systems. *Nonlinearity*, **16**, 521–557.

54 Grigoriev, R.O. and Schatz, M.F. (2006) Optically controlled mixing in microdroplets. *Lab Chip*, **6**, 1369.

55 Kroujiline, D. and Stone, H.A. (1999) Chaotic streamlines in steady bounded three-dimensional Stokes flows. *Physica D*, **130**, 105–132.

56 Neishtadt, A.I., Vainchtein, D.L., and Vasiliev, A. (2007) Adiabatic invariance in volume-preserving systems. in IUTAM Symposium on Hamiltonian Dynamics, Vortex Structures, Turbulence (eds. A.V. Borisov, V.V. Kozlov, I.S. Mamaev, and M.A. Sokolovskiy), pp. 89–108.

57 Solomon, T.H. and Mezic, I. (2003) Uniform, resonant chaotic mixing in fluid flows. *Nature*, **425**, 376–380.

58 Neishtadt, A.I. (2005) Capture into resonance and scattering on resonances in two-frequency systems. *Proceedings of the Steklov Institute of Mathematics*, **250**, 183–203.

59 Piro, O. and Feingold, M. (1988) Diffusion in three-dimensional Liouvillian maps. *Physical Review Letters*, **51**, 1709–1802.

60 Cartwright, J.H.E., Feingold, M., and Piro, O. (1995) Global diffusion in a realistic three-dimensional time-dependent nonturbulent fluid flow. *Physical Review Letters*, **75**, 3669–3672.

61 Cartwright, J.H.E., Feingold, M., and Piro, O. (1996) Chaotic advection in three-dimensional unsteady incompressible laminar flow. *Journal of Fluid Mechanics*, **316**, 259–284.